RAPID PREDICTION OF SOLID ROCKET IGNITION TRANSIENT PROCESS USING ARTIFICIAL NEURAL NETWORKS

by

Jian TENG[a], Zhenlong WU[b], Limei LU[c], and Yiqing LI[b*]

[a]School of Naval Architecture and Ocean Engineering, Guangzhou Maritime University, Guangzhou Jiaotong University (preparation), Guangzhou, China
[b]School of Aircraft Engineering, Nanchang Hangkong University, Nanchang, Jiangxi, China
[c]Shanghai Space Propulsion Technology Research Institute, Shanghai, Shanghai

Original scientific paper
https://doi.org/10.2298/TSCI240416176T

Solid rocket motors have been a critical component of space exploration, military operations, and numerous other applications for decades. The ability to accurately predict the ignition transient behavior of solid rocket motors is crucial for ensuring safe and reliable operations. In this study, ANN are employed to predict the ignition transient process of a model solid rocket motor. The training and validation data for the ANN are obtained through simulations of a validated quasi-1-D model. Results show that with the inputs of axial co-ordinate and igniting time, the ANN can predict density, axial velocity, temperature, and pressure in internal ballistic within 0.039 relative error and a correlation coefficient above 0.994 compared to the quasi-1-D simulations in millisecond level. With the increase of hidden layers and neural numbers in the ANN, prediction accuracy increases. When the hidden layers exceed four, prediction accuracy cannot improve significantly. When test data is out of the temporal range of the training and validation data, prediction accuracy decreases evidently. The trained ANN model can be used to predict solid rocket motors with increased internal ballistic spatial resolution within 0.007 relative error and to predict solid rocket motors with increased temporal resolution within 0.107 relative error.

Key words: *solid rocket motor, ignition transient, quasi-1-D model, machine learning, ANN*

Introduction

Solid rocket ignition is a complex process that involves a sequence of events leading to the propagation of the flame and combustion products within the rocket internal ballistic [1-3]. The ignition process is characterized by multiple transient phenomena that significantly influence the performance and operation of the rocket [4, 5]. These transient phenomena include hot gas formation, pressure rise, thrust development, and propagation of the flame front through the propellant. Accurate prediction of these characteristics is essential for the design and optimization of solid rocket motors, as well as for ensuring their safe and reliable operation [6, 7].

*Corresponding author, e-mail: yiqingli@nchu.edu.cn

Conventionally, predicting solid rocket ignition transient characteristics requires detailed modelling based on physical laws and empirical relations [2, 4, 5]. These models often consider complex events involving fluid dynamics, heat transfer, chemical reactions, and material properties [8, 9]. Large number of detailed models have been implemented into 2-D and 3-D CFD solvers for in-depth ignition transient analysis [10-13]. Although the detailed models show promising results to explore the physical mechanisms of pressure wave transportation, flame propagation, heat conduction and so on, the computation expenses are still huge [14, 15]. In rocket preliminary design phrase, rapid prediction models are sometimes more practical than accurate models. These rapid models either use empirical expressions or 0-D, 1-D analysis to quickly establish the relations between rocket geometry, grain installation, internal ballistic and thrust-time history [2, 4]. Several rapid prediction models for ignition transient evaluation have been developed. The model assumes that the pressure and temperature in the internal ballistic were uniform. Therefore, such models can not account for the geometry-dependent burning rate and flame propagation rate [16]. For the solid propellant motors with complex grain shapes, the predicted values of these models differ greatly from the experimental results. Meanwhile, for the commonly used solid rocket, this model is difficult to accurately predict the complex flame propagation process and the interaction between flow and combustion [17]. However, in the early prediction of solid rocket motor the simple model played a rapid role in estimating the moment of ignition and the stage of pressure rise [18]. Another rapid model, namely the model was also developed. In this model, the distribution of pressure, temperature and velocity along the grain is considered at every moment in the process. A series of control volume elements are established along the grain axis, and their increment is described by 1-D steady flow conservation equation. In the model, the changes of flow and burning surface area and the burning rate of the grain in axial direction can be considered [19]. However, the flame propagation rate is an input to the model and the induced ignition delay is usually not considered. Flame propagation can be treated in a variety of ways: as a time function determined by the test, as a linear function of the burning rate with time. Propulsion at a constant average rate, calculated according to the test pressure-time data, the combustion rate varies axially over the propellant surface by using a function calculated for the change of heat flux with gas temperature or boundary layer development [20]. Although model has been used for rapid internal ballistic evaluation of solid rocket motors, its utility is limited. Like the model, the model does not take into account the control of the igniting process, the flame spread rate, and the driving forces that depend on the shape of the grain surface [21]. Both the lumped analysis model and the quasi-1-D flow space model are difficult to accurately simulate the ignition transient and pressure rise process of solid rocket motors with high volume loading density, large throat area ratio and large length-diameter ratio configurations. These solid rocket motors are characterized by high internal gas velocities (Mach number > 0.3), significant axial pressure and temperature gradients, injection pressure, and relatively short ignition transient times [3, 22]. The motor's entire combustion chamber characteristics cannot be uniform for this kind of motor, nor can their change be managed in a quasi-steady state assumption, if the ignition transient and pressure rise process are to be expected. In order to overcome the ineffectiveness of the above two models, Peretz *et al*. [23] proposed model. The model takes into account the variation of the flow field and pressure with time and axial position, and the interaction between the developing flow field, the convective heat transfer of solid propellant, the flame propagation and the erosive combustion processes. The model is still a widely used model for fast prediction of the igniting and pressure rise phase. Beyond those improvement, the traditional rapid prediction models are highly sensitive to modelling assumptions and require precise parameterization for accurate predictions.

Additionally, the high dimensionality and non-linearity of the problem still leave accurate predictions using traditional numerical techniques challenging.

Data-driven techniques such as ANN offer an alternative approach for predicting solid rocket ignition transient characteristics [24-26]. By learning flow features from historical data, ANN can capture complex relationships that are difficult to model using traditional physical models. The ANN also provide a framework for incorporating multiple sources of data, including sensors readings, propellant properties, and environmental conditions [27, 28]. This integration allows for a more comprehensive prediction of transient characteristics that considers various interacting factors simultaneously [29, 30]. The consistently development of data-driven techniques provides new possibilities for rocket science in supplement of traditional method and solves the problems in a more efficient way.

In this paper, we propose the use of ANN to predict the ignition transient process of solid rocket motors. We aim to develop a ANN algorithm that can accurately capture the behavior of the ignition and grain burning system based on historical data. The model will be trained and validated using a large dataset obtained from quasi-1-D numerical simulations. The main objective of this study is to demonstrate the feasibility and effectiveness of using the rapid prediction ANN algorithm to predict ignition transients in solid rocket motors. The developed model can serve as a fast assessment tool for rocket motor design and optimization. By leveraging the capabilities of ANN, we aim to address the challenges associated with predicting ignition transients using traditional numerical methods and pave the way for more accurate and efficient predictions in the future.

Physical model and theoretical background

Schematic of solid rocket motor

The solid rocket motor configurations are reproduced from Tahsini [4]. Figure 1 shows a schematic of the solid rocket motor, which consists mainly of an igniter, propellant grain, and a Laval nozzle. The origin of the axial co-ordinate is set at the installation position of the igniter port. The grain is a simple tube configuration. The control volume inside the propellant has one inflow and one outflow boundary. The mass and heat release of propellant burnt gas is added into the control volume through source terms in the governing equations. The spatial resolution for each control volume is Δx and the control volume in the nozzle only has inflow and outflow boundaries without propellant burning.

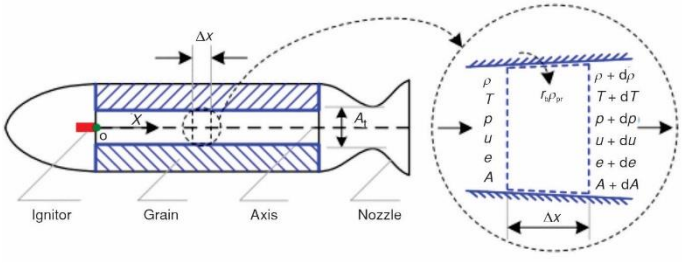

Figure 1. Schematic of solid rocket motor

Quasi-one-dimensional model

A quasi-1-D model is established to simulate the solid rocket motor ignition process. Two assumptions are made based on the physical process of the ignition transient process. First,

the ignition transient period is very short in the framework of the entire solid rocket work duration. Only a relatively thin layer of grain is burnt, thus grain regression is not considered. The internal ballistic flow area and burning surface perimeter remains unchanged during the ignition transient process. Second, the burnt gas of the grain is considered as ideal gas and the gas properties obeys the ideal gas state equation. Based on above assumptions, the governing equations for the quasi-one dimensional model are given by:

$$\frac{\partial(\rho A)}{\partial t}+\frac{\partial(\rho u A)}{\partial x}=r_{\mathrm{b}}P_{\mathrm{b}}\rho_{pr} \tag{1}$$

$$\frac{\partial(\rho u A)}{\partial t}+\frac{\partial\left[\left(\rho u^2+p\right)uA\right]}{\partial x}=p\frac{\mathrm{d}A}{\mathrm{d}x}+r_{\mathrm{b}}P_{\mathrm{b}}\rho_{pr}u_e \tag{2}$$

$$\frac{\partial(\rho E A)}{\partial t}+\frac{\partial\left[\left(\rho E+p\right)uA\right]}{\partial x}=r_{\mathrm{b}}P_{\mathrm{b}}\rho_{pr}h_{pr} \tag{3}$$

$$E=\frac{p}{\gamma-1}+\frac{1}{2}u^2 \tag{4}$$

where t and x are simulation time and axial co-ordinate, respectively, ρ – the density of burning gas, u – the axial velocity, A – the cross-section area of the internal ballistic, p – the pressure, E – the total energy, and γ – the specific heat ratio. For the propellant, r_{b} is the burning rate, P_{b} – the burning surface perimeter, ρ_{pr} – the density of propellant, u_e – the ejection velocity of the burning gas leaving the propellant surface, and h_{pr} – the enthalpy of the propellant. The burning rate for propellant is given by: $r_{\mathrm{b}}=A_{\mathrm{b}}p^{n_{\mathrm{b}}}$, where, A_{b} and n_{b} are two rate constants.

The 1-D heat conduction, eq. (5), in the solid propellant is solved to obtain the temperature distributions over grain surface. Here, κ is the heat conduction coefficient and h_{w} is the direction coordinate with the origin on the propellant surface and the direction vector perpendicular to grain surface. In our simulations, 100 ghost grid points are assigned along h_{w} direction for each control volume and the spatial resolution is 0.0002 m to resolve the temperature distributions inside the propellant. The properties of the model rocket motor are given in tab. 1:

$$\frac{\partial T}{\partial t}=\kappa\frac{\partial^2 T}{\partial h_{\mathrm{w}}} \tag{5}$$

Table 1. Properties of the model rocket motor [4]

Property	Value	Property	Value
Motor diameter	0.14 [m]	A_{b}	0.004 [ms^{-1}]
Initial grain diameter	0.1 [m]	n_{b}	0.4
Grain length	1.00 [m]	ρ_{pr}	1700 [kgm^{-3}]
Nozzle throat diameter	0.06 [m]	R	318 [Jkg^{-1}K^{-1}]
Nozzle exit diametet	0.12 [m]	γ	1.21
h_{pr}	6.8×10^6 [Jkg^{-1}]	u_e	180 [ms^{-1}]
κ	1.28 [Wm^{-1}K^{-1}]	$T_{\mathrm{w},\infty}$	300 [K]

The temporal variations of mass-flow rate and gas temperature from igniter are given as inflow boundary conditions for the equation system. The two values are fitted through the

igniter mass and temperature curves form Tahsini [4] and are given in the form of piecewise function in our code as shown in eqs. (6) and (7). The coefficients of the igniter model are shown in tab. 2:

$$T_{ig} = \begin{cases} \dfrac{c_{a1}}{1+\mathrm{e}^{\left[c_{a2}(t-c_{c3})\right]}} & t \le 0.033 \\ c_{b1}t^{c_{b2}} + c_{b3}t^{c_{b4}} & t > 0.033 \end{cases} \tag{6}$$

$$\dot{m}_{ig} = \begin{cases} \dfrac{c_{c1}}{1+\mathrm{e}^{\left[c_{c2}(t-c_{c3})\right]}} + c_{c4} & t \le 0.033 \\ \mathrm{e}^{\left(c_{d1}+c_{d2}t^3+\frac{c_{d3}}{t^{1.5}}\right)} & t > 0.033 \end{cases} \tag{7}$$

Table 2. Coefficients of the igniter model

Coefficient	Value	Coefficient	Value
c_{a1}	2468.293	c_{c1}	5.9257505
c_{a2}	5756.564	c_{c2}	–334.7422
c_{a3}	0.000615	c_{c3}	–0.003320
c_{b1}	0.070999	c_{c4}	–4.381228
c_{b2}	–2.987889	c_{d1}	–7.828060
c_{b3}	516.7691	c_{d2}	–16470.401
c_{b4}	0.248223	c_{d3}	0.0491065

The governing equations were discretized using the finite difference method [31]. For the splitting of the inviscid fluxes, the Van Leer method was employed [32]. The inviscid fluxes were solved using the WENO5 method [33], which is a fifth-order weighted essentially non-oscillatory scheme. The heat conduction equation was solved using a fourth-order central difference scheme. Finally, the time advancement was performed using a third-order Runge-Kutta method [34]. The quasi-1-D solver is an in-house code, written in the Fortran programming language, and operates in a serial mode.

Two metrics, namely the relative error, $E_r(v)$, and correlation coefficient, $C_r(v)$, are adopted to evaluate the difference between the model prediction and the true value. Those two metrics are also used to evaluate the accuracy of ANN mode predictions and the quasi-1-D model simulations. The definitions for the two metrics are given, respectively. Here, the $\langle\cdot\rangle$ represents ensemble average operation:

$$E_r(v) = \frac{\left\langle \left(v^{\text{real}} - v^{\text{model}}\right)^2 \right\rangle^{1/2}}{\left\langle \left(v^{\text{real}}\right)^2 \right\rangle^{1/2}},\ C_r(v) = \frac{\left\langle \left(v^{\text{real}} - \left\langle v^{\text{real}} \right\rangle\right)\left(v^{\text{model}} - \left\langle v^{\text{model}} \right\rangle\right) \right\rangle}{\left\langle \left(v^{\text{real}} - \left\langle v^{\text{real}} \right\rangle\right)^2 \right\rangle^{1/2} \left\langle \left(v^{\text{model}} - \left\langle v^{\text{model}} \right\rangle\right)^2 \right\rangle^{1/2}} \tag{7}$$

Figure 2 shows the pressure history at internal ballistic head from reference data [4] and simulations of the quasi-1-D model. In fig. 2(a), three sets of grid are tested for grid convergence study using identical time step size ($\Delta t = 1\times10^{-7}$ seconds). It is shown that with the increase of axial grid points from 400 to 1200, the pressure history gradually converges and coincide with the reference data. The results from quasi-1-D simulations with grids of 800 and 1200 nearly overlap with each other, suggesting that the grid converges with axial grid number

exceed 800. Figure 2(b) shows the pressure history simulated with fixed axial grid number (N_x = 800) and three different time step size. It is shown that with the decrease of time step size from $\Delta t = 1\times10^{-7}$ seconds to $\Delta t = 1\times10^{-8}$ seconds, the pressure history curves overlap with each other, indicating that time step size has little influence on the simulation results when $\Delta t \leq 1\times10^{-7}$ seconds.

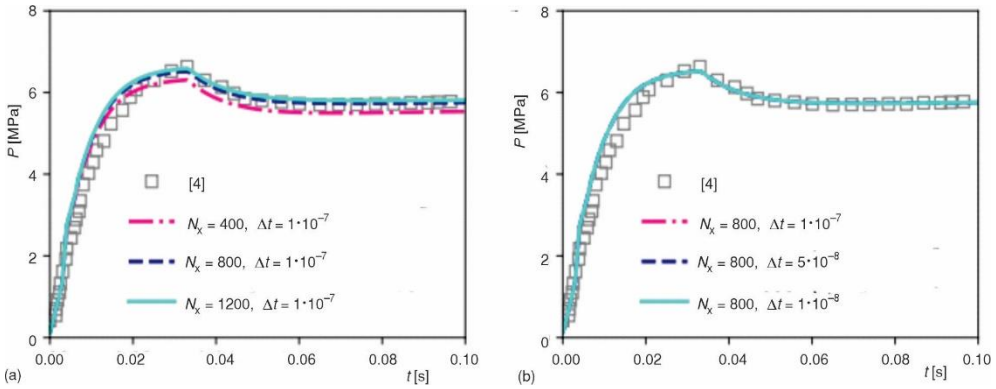

Figure 2. Pressure history at internal ballistic head

Table 3 presents the relative errors and correlation coefficients statistics from quasi-1-D simulations in comparison withe the reference data [4]. It can be found that with the increase of grid resolutions, the relative error deceases from 0.051 to 0.044 and the correlation coefficients increase from 0.977 to 0.983. When the time step size decreases from 1×10^{-7} seconds to 1×10^{-8} seconds, the two metrics for simulations with axial grid points of 800 do not change evidently. The above results demonstrate that the simulation results converge when the axial grid points exceed 800 and the time step size $\Delta t \leq 1\times10^{-7}$ seconds. The simulation data under previous conditions can be used to train and validate the ANN model.

Table 3. Relative errors and correlation coefficients statistics from quasi-1-D simulations

No.	Grid No.	Δt	$E_r(p)$	$C_r(p)$
1	400	$\Delta t = 1\times10^{-7}$ s	0.051	0.977
2	800	$\Delta t = 1\times10^{-7}$ s	0.048	0.982
3	1200	$\Delta t = 1\times10^{-7}$ s	0.044	0.983
4	800	$\Delta t = 5\times10^{-8}$ s	0.044	0.982
5	800	$\Delta t = 1\times10^{-8}$ s	0.044	0.982

Architecture of the ANN model

An ANN is a computational model that simulates the way the human brain processes information. It consists of an input layer that receives raw data, one or more hidden layers that extract features and create complex patterns through interconnected neurons, and an output layer that generates the final prediction or decision. The network learns by adjusting the weights and biases of its neurons through a training process involving backpropagation, which iteratively minimizes the error between the network's predictions and the actual outcomes. This adaptive learning allows ANN to capture non-linear relationships and perform tasks such as classification, regression, and pattern recognition with high accuracy. The architecture of the ANN model in current study is shown in fig. 3. The variables feed into the input layer are axial

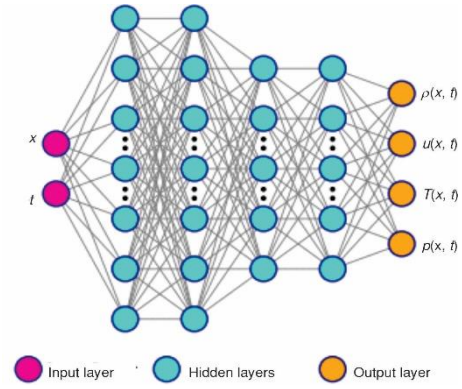

Figure 3. Architecture of the ANN model

location x and the ignition time, *t*. Four variables, namely, density, ρ , axial velocity, *u*, temperature, *T*, and pressure, *p*, constitute the output layer. The hidden layers connect the input layer and the output layer and the number of hidden layers and the number of neurons in each hidden layer can be modified and tested in subsequent study. The sinusoidal is chosen as the activation function for the hidden layers. The batch size and the learning rate for the ANN model are 10000 and 0.001, respectively. The mean square error loss function is selected to measure the performance and accuracy of the ANN model. For each case, the training and validation data are first packed together in random order in one data file. This data file consisted of six columns. The first two columns are the input variables and the rest four columns are the output variables. In training and validation procedure, the data file is split into two separate files containing training data and validation data in a ratio of 7:3. During the ignition transient period, the values of flow variables, especially the values of temperature, and pressure, change evidently. Thus, to obtain a generalized input and output, as well as to improve the robustness of the ANN model, both inputs and outputs are normalized using the ensemble average and standard deviation values. The normalizations of input and output layers are given by: $v^{\text{norm}} = (v - v^{\text{avg}})/v^{\text{std}}$. The previous ANN network was constructed using the open-source software TensorFlow [35].

Results and discussions

Influence of ANN hidden layer structures

Four ANN models with different hidden layer structures are first tested. The training and validation data in this subsection are from quasi-1-D simulations with spatial resolution $N_x = 800$ and temporal resolution $\Delta t = 1\times10^{-7}$ seconds. The overall training and validation data are packed using solution instants saved at every 0.0001s and thus the total data packed are solutions are 1000 time instants. The four ANN models have identical inputs and outputs, but different hidden layers. For example, (20,10) represents a ANN model with two hidden layers and the first hidden layer has 20 neurons while the second hidden layer has 10 neurons. The number of hidden layers of the four ANN models increase from 2 to 5. The prediction accuracy of the four ANN models is shown in tab. 4. It can be found that with the increase of hidden layers and the number of neurons in each hidden layer, the relative errors for pressure decrease from 0.039 to 0.007 and the correlation coefficients increase from 0.994 to 0.999. While the relative errors for temperature decrease from 0.068 to 0.006 and the correlation coefficients increase from 0.948 to 0.999. For ANN models with 4 and 5 hidden layers, the prediction accuracy are very close to each other, indicting that the prediction accuracy can not improve significantly with the increase of hidden layer and the number of neurons in each hidden layer when hidden layers exceed 4. Simulating the ignition process of a solid rocket using quasi-1-D model takes approximately 4 minutes, whereas the computation time using an ANN is less than 0.3 seconds.

Figure 4 shows the temporal variations of pressure and temperature predicted by ANN model with different hidden layer structures. It can be observed that the predictions by (20,10) and (20,40,10) models deviate from the quasi-1-D model simulations during the ignition transient

process at $t > 0.02$ seconds. The predictions by (20,40,40,10) and (20,40,80,40,10) models coincide with the quasi-1-D model simulations during the entire ignition transient process.

Table 4. Prediction accuracy of ANN models.

ANN structure	$E_r(p)$	$C_r(p)$	$E_r(T)$	$C_r(T)$	CPU-time [s]
(20,10)	0.039	0.994	0.068	0.948	0.107
(20,40,10)	0.020	0.998	0.018	0.996	0.183
(20,40,40,10)	0.008	0.999	0.007	0.999	0.211
(20,40,80,40,10)	0.007	0.999	0.006	0.999	0.284

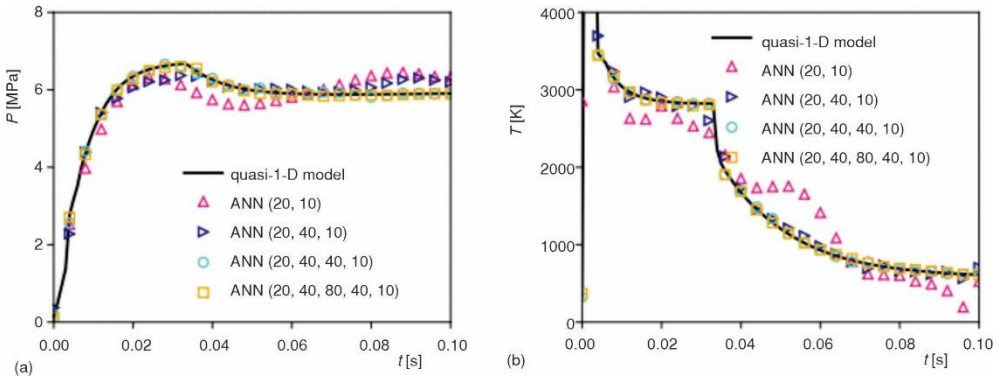

Figure 4. Temporal variations of pressure and temperature predicted by ANN model with different structures

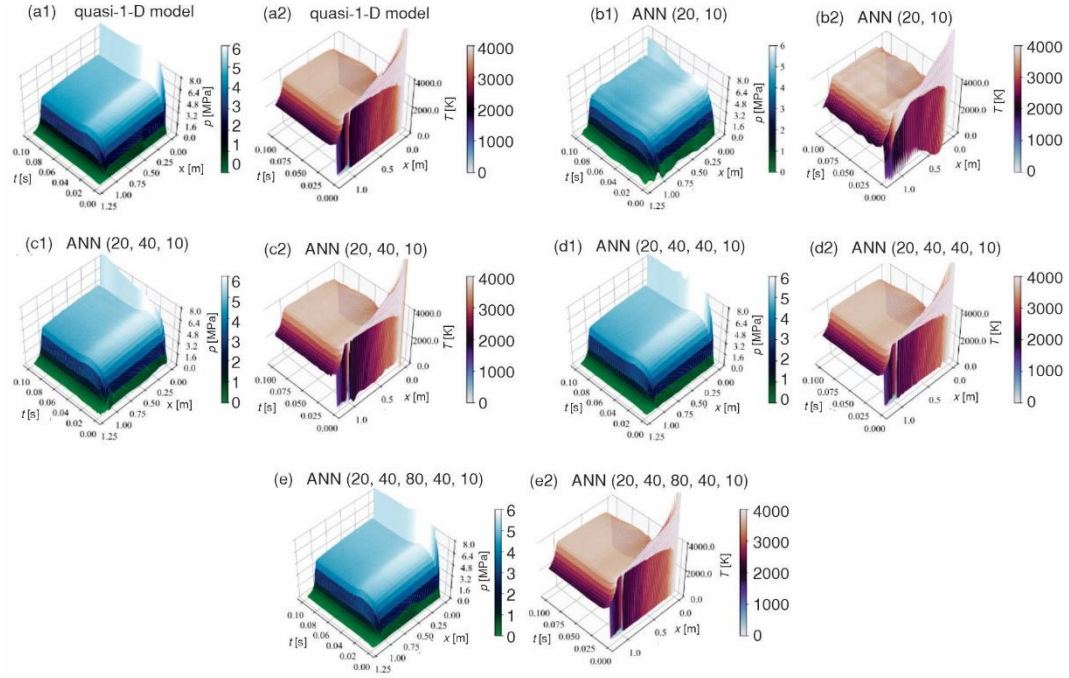

Figure 5. Spatial-temporal variations of pressure and temperature prediction by quasi-1-D model and different ANN models

Figure 5 shows spatial-temporal variations of pressure and temperature prediction by quasi-1-D model and different ANN models. It can be found that the spatial-temporal variations of pressure and temperature predicted by (20,10) and (20,40,10) models only capture the variable distributions in middle part of the rocket internal ballistic. The variable distributions near the head region predicted by those two models greatly different form the quasi-1-D model simulation. The predictions by (20,40,40,10) and (20,40,80,40,10) models can properly recovery the spatial-temporal variations of pressure and temperature during the ignition transient process.

To check more details of the ANN model predictions, the spatial distributions of pressure and temperature at two instants are shown in figs. 6 and 7, respectively. At the first few

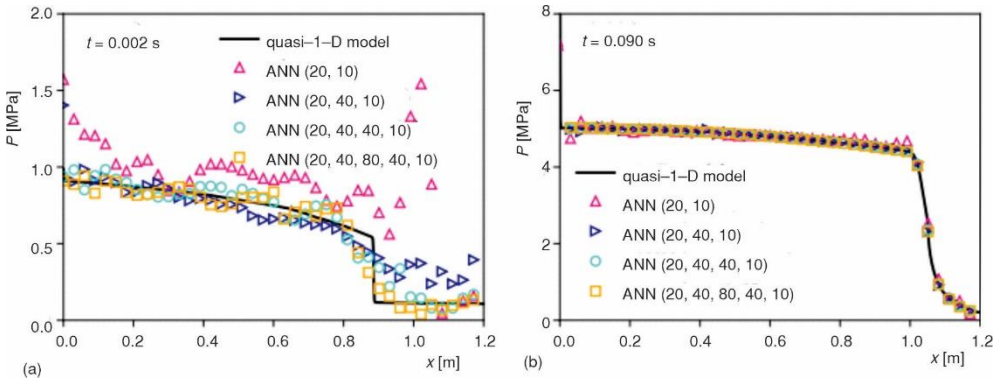

Figure 6. Spatial distribution of pressure at t = 0.002 seconds and 0.090 seconds from different ANN models

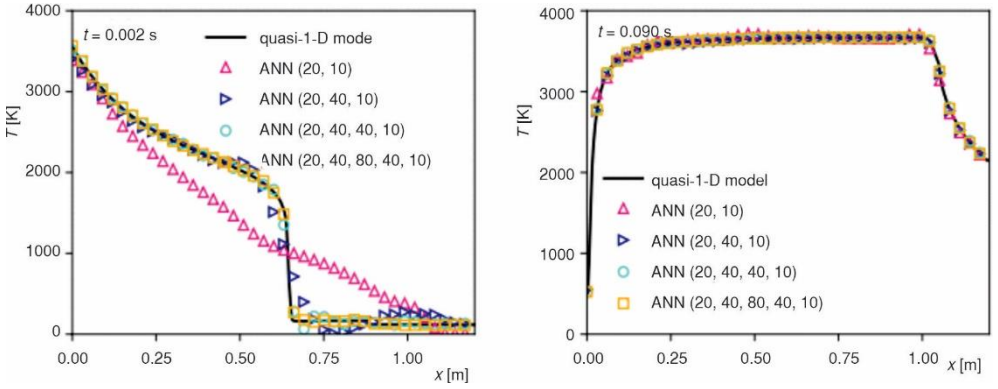

Figure 7. Spatial distribution of temperature at t = 0.002 seconds and 0.090 seconds from different ANN models

milliseconds of ignition, the values of flow variables in the internal ballistic change very quickly. At t = 0.002 seconds as shown in fig. 6(a), the high pressure gas released from igniter gradually raise the pressure level in the internal ballistic. It is shown that the predictions by (20,10) and (20,40,10) models can not properly capture the instant pressure distributions in the internal ballistic while the predictions by (20,40,40,10) and (20,40,80,40,10) models can reasonably recovery the instant pressure distributions but with poor accuracy. At t = 0.090 seconds, approaching the end of ignition transient period, the pressure distributions predicted by four ANN models can coincide with the quasi-1-D simulation. The ANN model predictions of temperature as shown in fig. 7 are quite similar to the predictions of pressure. The reason for the poor

predictions of pressure and temperature at the first few milliseconds by ANN models can be attribute to the fact that at the very beginning of ignition transient, the pressure and temperature in internal ballistic instantly increase form atmospheric conditions to the igniter hot gas condition, the changes are very fast and the values varies greatly. The training and validation data are inadequate for the ANN models to learn those transient feature.

Influence of training data

The datasets used for ANN training and validation are simulations results by quasi-1-D model ranging from 0 to 0.1 seconds. In this subsection, the training and validation data are tailored to assess the extrapolation potential of the ANN model. Four groups of training and validation datasets are prepared as shown in tab. 5. The 20% data suggests that the training and validation data only cover the first 20% of the entire dataset during the ignition transient process, which contains quasi-1-D simulations form 0-0.02 seconds. The 40%, 60%, and 80% data are packed according to the same principal. After the training and validation, the models are used to predict the variable variations during the entire ignition transient process from 0-0.1 seconds. As shown in tab. 5, the relative error of ANN model predictions gradually decrease with the increase of training and validation data length while the correlation coefficients increase slightly. The results suggest that with the increase of training and testing data length, the prediction accuracy of ANN model can be improved in relative extent.

Table 5. Prediction accuracy of ANN model with different training data length.

Datasets	$E_r(p)$	$C_r(p)$	$E_r(T)$	$C_r(T)$
20% data	0.930	0.028	0.833	0.083
40% data	0.772	0.046	0.658	0.192
60% data	0.765	0.057	0.654	0.223
80% data	0.758	0.101	0.628	0.242

To find more details of the performance of the ANN model trained and validated with different data length, the spatial distributions of pressure and temperature at two time instants are shown in figs. 8 and 9, respectively. It can be found that for pressure and temperature distributions at t = 0.002 seconds as shown in figs. 8(a) and 9(a), the predictions by ANN models trained and tested with different data length can properly recovery the transient features compared to simulations by quasi-1-D model. However, the pressure and

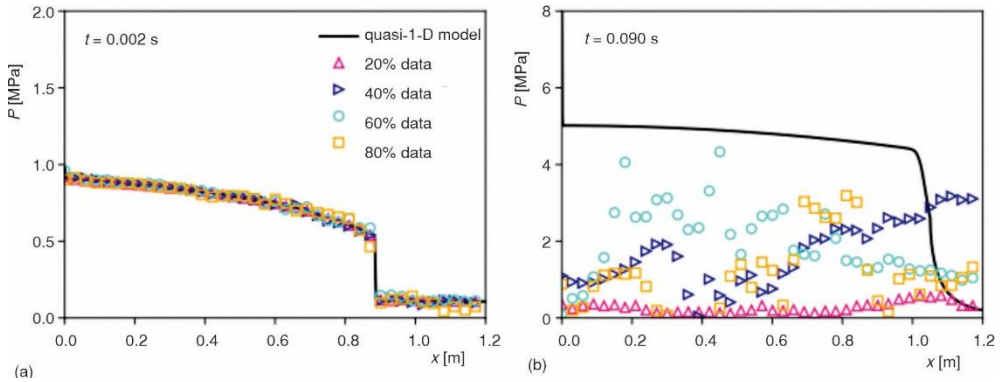

Figure 8. Spatial distribution of pressure at t = 0.002 seconds and 0.090 seconds from ANN model trained by different data length

temperature distributions at t = 0.090 seconds greatly deviate from the quasi-1-D model simulations as shown in figs. 8(b) and 9(b). The results indicate that when the predictions data is out of the temporal range of training and validation data, the extrapolation capability for the ANN model is poor.

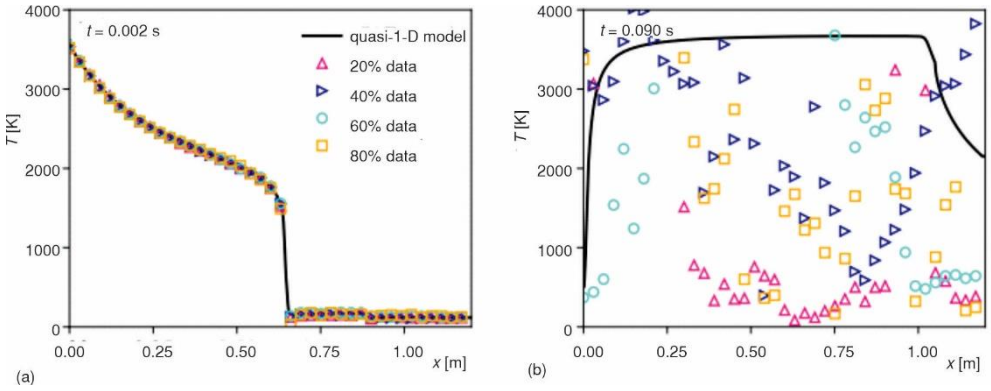

Figure 9. Spatial distribution of temperature at t = 0.002 seconds and 0.090 seconds from ANN model trained by different data length

Prediction of increased spatial resolution

In previous subsections, the quasi-1-D simulation of N_x = 800 and $\Delta t = 1\times10^{-7}$ results are used to train and validate the ANN model. The training and validation data are saved at $tr = 1\times10^{-4}$, which contains 1000 instant solution data in the ignition transient process. To test the capability of the ANN model in predicting the increased spatial resolution, N_x = 900, 1000, 1100, and 1200 are tested using ANN model trained by N_x = 800 datasets. Table 6 presents the prediction accuracy of these results. It is shown that with the increase of spatial resolution from 900 to 1200, the relative errors of pressure and temperature are between 0.006 and 0.007, while the correlation coefficients of pressure and temperature are above 0.998. The results indicate that the ANN model has good performance in predicting the ignition transient process with increased spatial resolution using model trained in a lower spatial resolution datasets.

Table 6. Prediction accuracy with increase spatial resolution.

Spatial resolution	$Er(p)$	$Cr(p)$	$Er(T)$	$Cr(T)$
N_x = 900	0.006	0.999	0.006	0.999
N_x = 1000	0.006	0.999	0.006	0.999
N_x = 1100	0.007	0.998	0.006	0.999
N_x = 1200	0.007	0.998	0.006	0.998

Figure 10 shows the temporal variations of pressure and temperature predicted with increased spatial resolutions. It can be found that with the increase of spatial resolution, the ANN predicted pressure slightly increase and the ANN predicted temperature slightly decrease at $t \geq 0.04$ seconds. Overall, the ANN model predictions are in good agreement with quasi-1-D simulations.

Figure 11 shows spatial-temporal variations of pressure and temperature predicted with N_x = 1200 using ANN model and quasi-1-D simulation. It is shown that the results are quite similar to each other, suggesting that the capability of ANN model in predicting increased spatial resolution is fairly good.

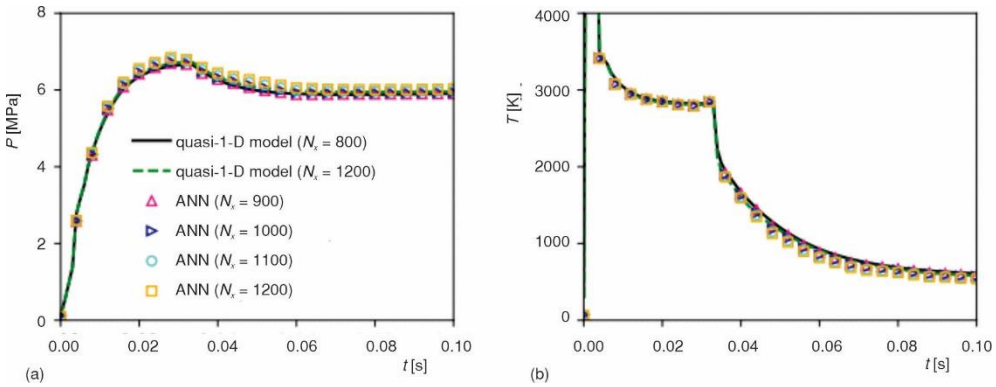

Figure 10. Temporal variations of pressure and temperature predicted with increased spatial resolutions

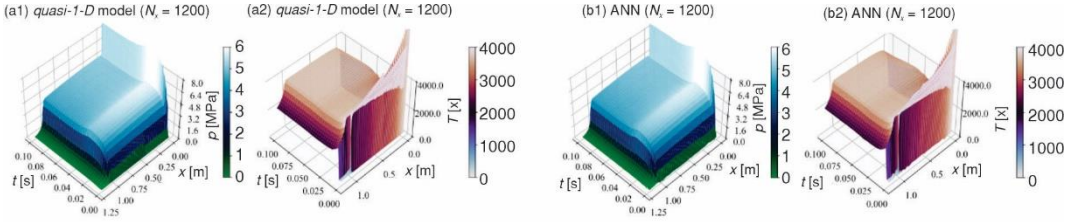

Figure 11. Spatial-temporal variations of pressure and temperature predicted with N_x = 1200

Prediction of increased temporal resolution

Additionally investigated is the ANN model's capacity to forecast higher temporal resolution. The prediction accuracy of the ANN model in predicting results with higher temporal resolution is displayed in tab. 7. It is discovered that as temporal resolution increases, the correlation coefficient of pressure slightly decreases and the relative errors of temperature and pressure steadily increase. The findings imply that the ANN model's predictive power for higher temporal resolution results is inferior to its predictive power for higher spatial resolution results.

Table 7. Prediction accuracy with increase temporal resolution.

Temporal resolution [s]	*Er*(*p*)	*Cr*(*p*)	*Er*(*T*)	*Cr*(*T*)
$tr = 1\times10^{-7}$	0.088	0.960	0.020	0.998
$tr = 5\times10^{-8}$	0.096	0.956	0.021	0.998
$tr = 1\times10^{-8}$	0.107	0.953	0.021	0.998

Figure 12 shows the spatial-temporal (0.0026 seconds < t < 0.0034 seconds) contours of pressure predicted with increased temporal resolutions. During this period, the values of pressure in the internal ballistic change evidently. As shown in the fig. 12(a2) for predicting contour using a temporal resolution of $tr = 1\times10^{-7}$, the pattern of high pressure and low pressure regions are comparable with the quasi-1-D simulation as shown in fig. 12(a1). However, the division of high pressure and low pressure is not as clear as the quasi-1-D simulation. With the increase of temporal resolution as shown in figs. 12(b2) and 12(c2), the pattern of high pressure and low pressure region are obscure and the division of high pressure and low pressure are not as clear as those obtained by quasi-1-D simulations. The results demonstrate that the temporal interpolation ability of the ANN model is not as good as its spatial interpolation capability.

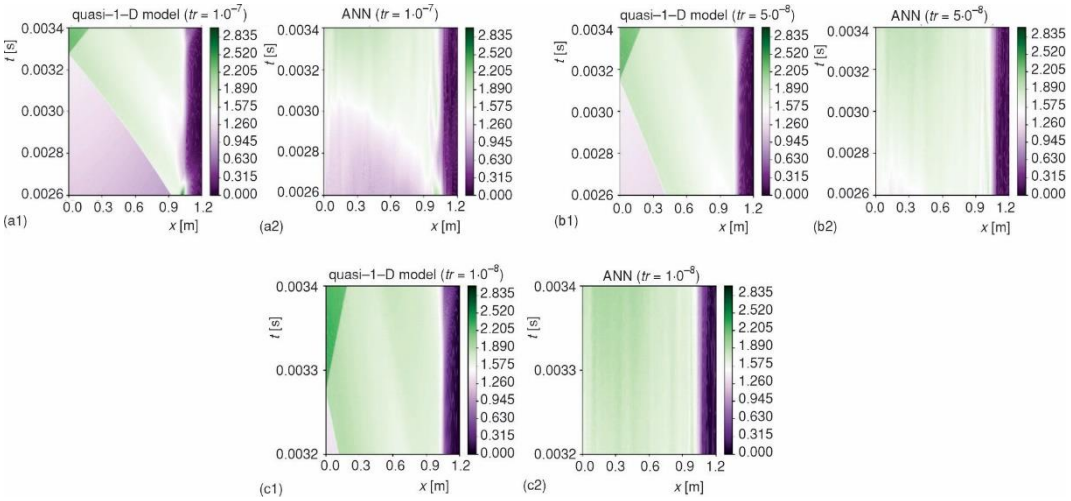

Figure 12. Spatial-temporal (0.0026 seconds < *t* < 0.0034 seconds) contours of pressure predicted with increased temporal resolutions

Conclusions

In this study, we have delved into the prediction of solid rocket ignition transients, a complex phenomenon involving the ignition of propellant grains, the subsequent rise in internal ballistic pressure, and temperature elevation. To address this, we first established a quasi-1-D model that captured the essential physics of solid rocket ignition. This model was validated against data from reference studies, confirming its accuracy and reliability.

Subsequently, we constructed a fully connected ANN model, utilizing the quasi-1-D model's simulated data as training and validation database. The ANN model took time and internal ballistic axial position as inputs, and predicted transient density, velocity, temperature, and pressure as outputs. The model's performance was then tested by varying its architecture, specifically the number of hidden layers and neurons within each layer. Our findings indicated that as the complexity of the ANN architecture increased, so did its prediction accuracy. Notably, when the model had four hidden layers, the relative error of predictions was less than or equal to 0.008, with a correlation coefficient of at least 0.999. However, adding more than four hidden layers did not lead to further significant improvements.

To assess the ANN extrapolation capabilities, we trained it using datasets with varying simulation durations. The results showed that the ANN was highly accurate in predicting data within the training duration range but exhibited lower accuracy when extrapolating beyond this range. This observation highlighted thelimitations of the ANN extrapolation abilities. To further explore the ANN performance, we tested its prediction on data with higher spatial and temporal resolutions. Interestingly, while the model maintained good accuracy for increased spatial resolution, its performance suffered a slight decrease when dealing with higher temporal resolution data. The ANN model developed in this study has demonstrated promising results in predicting solid rocket ignition transients. Its accuracy, particularly when using four hidden layers, is sufficient for practical applications. However, it is important to note that the model's extrapolation capabilities are limited, and further study is needed to improve its performance in this area. Additionally, future studies could investigate techniques to enhance the ANN ability to handle data with varying temporal resolutions. This work represents a step forward in ANN based

modelling of solid rocket ignition transients and lays the foundation for more advanced and accurate predictions in rocket science.

Acknowledgment

This work was supported by Guangdong Basic and Applied Basic Research Foundation through Grant No. 2021A1515110845 and Start-up Fund for Talent Introduction at Guangzhou Jiaotong University through Grant No. K42024014.

Nomenclature

A – internal ballistic area, [m^2]
A_b – grain burning rate coefficient, [–]
$Cr(v)$ – correlation coefficient of variable, [–]
E – rocket gas total energy, [J]
$Er(v)$ – relative error of variable, [–]
h_{pr} – enthalpy of the grain, [Jkg^{-1}]
h_w – grain wall normal co-ordinate, [m]
$\dot{m}_{ig}$ – igniter gas mass-flow rate, [kgs^{-1}]
n_b – grain burning rate coefficient, [–]
P_b – grain burning surface perimeter, [m]
p – rocket gas pressure, [Pa]
R – rocket gas constant, [Jkg^{-1}K^{-1}]
r_b – grain burning rate, [ms^{-1}]
T_{ig} – igniter gas temperature
$T_{w,\infty}$ – grain wall temperature at remote distance, [K]
t – simulation time, [s]
u – rocket gas axial velocity, [ms^{-1}]
u_e – burnt gas ejection speed, [ms^{-1}]
x – axial co-ordinate, [m]

Greek symbols

γ – specific heat ratio of rocket gas, [–]
κ – grain heat conduction coefficient, [Wm^{-1}K^{-1}]
ρ – rocket gas density, [kgm^{-3}]
ρ_{pr} – grain density, [kgm^{-3}]

References

[1] Summerfield, M., *Solid Propellant Rocket Research*, American Institute of Aeronautics and Astronautics, New York, USA, 1960
[2] d'Agostino, L., *et al*., An Ignition Transient Model for Solid Propellant Rocket Motors, *Proceedings*, 37th Joint Propulsion Conference and Exhibit, Salt Lake City, Ut., USA, 2001
[3] Vr Sanal Kumar, Raghunandan, B., Ignition Transient of Dual-Thrust Solid Propellant Rocket Motors – A Review, *Proceedings*, 48th AIAA/ASME/SAE/ASEE Joint Propulsion Conference & Exhibit, Atlanta, Geo., USA, 2012
[4] Tahsini, A. M., Ignition Transient Simulation in Solid Propellant Rocket Motors, *Proceedings*, 45th AIAA Aerospace Sciences Meeting and Exhibit, Reno, Nev., USA, 2007
[5] Francois, L., *et al*., A New Simulation Strategy for Solid Rocket Motor Ignition: Coupling a CFD Code with a One-Dimensional Boundary Flame Model, Verification Against a Fully Resolved Approach, *Proceedings*, AIAA Propulsion and Energy 2021 Forum, VIRTUAL EVENT, American Institute of Aeronautics and Astronautics, Reston, Va., USA, 2021
[6] Pardue, B., Han, S., Ignition Transient Analysis of a Solid Rocket Motor Using a One Dimensional Two Fluid Model, *Proceedings*, 28th Joint Propulsion Conference and Exhibit, Nashville, Tenn., USA
[7] Li, Y., *et al*., Fluid-Structure Coupled Simulation of Ignition Transient in a Dual Pulse Motor Using Overset Grid Method, *Acta Astronautica, 183* (2021), June, pp. 211-226
[8] Cai, W., *et al*., A Model of AP/HTPB Composite Propellant Combustion in Rocket-Motor Environments. *Combustion Science and Technology, 180* (2008), 12, pp. 2143-2169
[9] Gieras, M., Gorgeri, A., Numerical Modelling of the Hybrid Rocket Engine Performance, *Propulsion and Power Research, 10* (2021), 1, pp. 15-22
[10] Hegab, A. M., *et al*., Numerical Modeling for the Combustion of Simulated Solid Rocket Motor Propellant, *Computers & Fluids, 89* (2014), Jan., pp. 29-37
[11] Ma, Y., *et al*., A Model for Igniter Mass-flow Rate History Evaluation for Solid Rocket Motors, *International Journal of Aerospace Engineering*, 2019, On-line first, https://doi.org/10.1155/2019/2593602
[12] Tola, C., Nikbay, M., Internal Ballistic Modeling of a Solid Rocket Motor by Analytical Burnback Analysis, *Journal of Spacecraft and Rockets, 56* (2019), 2, pp. 498-516
[13] Rohini, D., *et al*., Design & Analysis of Solid Rocket Using Open Rocket Software, *Materials Today: Proceedings, 64* (2022), Part 1, pp. 425-430

[14] Hartfield, R., *et al*., A Review of Analytical Methods for Solid Rocket Motor Grain Analysis, *Proceedings*, 39th AIAA/ASME/SAE/ASEE Joint Propulsion Conference and Exhibit, Huntsville, Ala., USA, 2003
[15] Hartfield, R., *et al*., Analytical Methods for Predicting Grain Regression in Tactical Solid-Rocket Motors. *Journal of Spacecraft and Rockets, 41* (2004), 4, pp. 689-693
[16] Kashiwagi, T., *et al*., Experimental Study of Ignition and Subsequent Flame Spread of a Solid Fuel in a Hot Oxidizing Gas Stream, *Combustion and Flame, 24* (1975), Feb., pp. 357-364
[17] Rasbash, D. J., A Flame Extinction Criterion for Fire Spread, *Combustion and Flame, 26* (1976), Feb., pp. 411-412
[18] Fernandez-Pello, A., Williams, F. A., A Theory of Laminar Flame Spread Over Flat Surfaces of Solid Combustibles, *Combustion and Flame, 28* (1977), Jan., pp. 251-277
[19] Alekseev, M. V., Averson, A. E., Mechanism of the Propagation of a Flame Over a Surface in a Counterflow of Gas, *Combustion, Explosion, and Shock Waves, 15* (1979), 5, pp. 594-600
[20] Sirignano, W. A., A Critical Discussion of Theories of Flame Spread across Solid and Liquid Fuels, *Combustion Science and Technology, 6* (1972), 1-2, pp. 95-105
[21] Fernandez-Pello, A. C., Flame Spread in a Forward Forced Flow, *Combustion and Flame, 36* (1979), Jan., pp. 63-78
[22] Sanal Kumar, V. R., *et al*., Starting Transient Flow Phenomena in Inert Simulators of Solid Rocket Motors with Divergent Ports, *Journal of Propulsion and Power, 22* (2006), 5, pp. 1138-1141
[23] Peretz, A., *et al*., Starting Transient of Solid-Propellant ocket Motors with High Internal Gas Velocities, *AIAA Journal, 11* (1973), 12, pp. 1719-1727
[24] Abreu, J., *et al*., A Comprehensive Approach to Predict a Rocket's Impact with Stochastic Estimators and Artificial Neural Networks, *IET Signal Processing, 15* (2021), 9, pp. 649-665
[25] Lee, H. S., *et al*., Neural Networks for the Burn Back Performance of Solid Propellant Grains, *Aerospace Science and Technology, 137* (2023), 108283
[26] Lee, H. S., *et al*., Optimization of a Solid Rocket Motor Design through Neural Network-Assisted Performance Prediction, *IEEE Transactions on Aerospace and Electronic Systems, 59* (2023), 6, pp. 8769-8781
[27] Jung, M. Y., *et al*., Dynamic Model and Deep Neural Network-Based Surrogate Model to Predict Dynamic Behaviors and Steady-State Performance of Solid Propellant Combustion, *Combustion and Flame, 250* (2023), 112649
[28] Lee, B. J., *et al*., Adaptive Osher-Type Scheme for the Euler Equations with Highly Nonlinear Equations of State, *Journal of Computational Physics, 246* (2013), Aug., pp. 165-183
[29] Williams, A., *et al*., A Machine Learning Approach for Solid Rocket Motor Data Analysis and Virtual Sensor Development, *Proceedings*, AIAA Propulsion and Energy 2020 Forum, VIRTUAL EVENT, American Institute of Aeronautics and Astronautics, Reston, Va., USA, 2020
[30] Hartfield, R. J., Carpenter, M., Statistical Learning for Solid Propellant Performance, *Proceedings*, AIAA Propulsion and Energy 2021 Forum, VIRTUAL EVENT, American Institute of Aeronautics and Astronautics, Reston, Va., USA, 2021
[31] Abell, M. L., Braselton, J. P., First-Order Ordinary Differential Equations, in: *Differential Equations with Mathematica*, Elsevier,Amsterdam, The Netherlands, 2016, pp. 45-131
[32] Clerc, S., Accurate Computation of Contact Discontinuities in Flows with General Equations of State, *Computer Methods in Applied Mechanics and Engineering, 178* (1999), 3-4, pp. 245-255
[33] Johnsen, E.,On the Treatment of Contact Discontinuities Using WENO Schemes, *Journal of Computational Physics, 230* (2011), 24, pp. 8665-8668
[34] Nasab, S. H., Vermeire, B. C., Third-Order Paired Explicit Runge-Kutta Schemes for Stiff Systems of Equations, *Journal of Computational Physics, 468* (2022), 111470
[35] Abadi, M., *et al*., Tensorflow: Large-Scale Machine Learning on Heterogeneous Distributed Systems, *Proceedings*, 12th USENIX Symposium on Operating Systems Design and Implementation (OSDI 16), Savannah, Geo., USA, 2016

Paper submitted: April 16, 2024
Paper revised: June 20, 2024
Paper accepted: July 2, 2024